



HAL
open science

Two fast integrators for the Galactic tide effects in the Oort Cloud

S. Breiter, Marc Fouchard, R. Ratajczak, W. Borczyk

► **To cite this version:**

S. Breiter, Marc Fouchard, R. Ratajczak, W. Borczyk. Two fast integrators for the Galactic tide effects in the Oort Cloud. *Monthly Notices of the Royal Astronomical Society*, 2007, 377, pp.1151-1162. 10.1111/j.1365-2966.2007.11654.x . hal-03730680

HAL Id: hal-03730680

<https://hal.science/hal-03730680>

Submitted on 6 Oct 2022

HAL is a multi-disciplinary open access archive for the deposit and dissemination of scientific research documents, whether they are published or not. The documents may come from teaching and research institutions in France or abroad, or from public or private research centers.

L'archive ouverte pluridisciplinaire **HAL**, est destinée au dépôt et à la diffusion de documents scientifiques de niveau recherche, publiés ou non, émanant des établissements d'enseignement et de recherche français ou étrangers, des laboratoires publics ou privés.

Two fast integrators for the Galactic tide effects in the Oort Cloud

S. Breiter,¹* M. Fouchard,^{2,3}* R. Ratajczak¹* and W. Borczyk¹*

¹*Astronomical Observatory of A. Mickiewicz University, Stoleczna 36, Poznań 60-286, Poland*

²*INAF–IASF Roma, Via del Fosso del Cavaliere 100, 00133 Roma, Italy*

³*IMCCE/SYRTE, Observatoire de Paris, 77 av. Denfer-Rochereau, 75014 Paris, France*

Accepted 2007 February 21. Received 2007 February 15; in original form 2006 July 10

ABSTRACT

Two fast and reliable numerical integrators for the motion of the Oort Cloud comets in the Galactic tidal potential are presented. Both integrators are constructed as Hamiltonian splitting methods. The first integrator is based upon the canonical Hamiltonian equations split into the Keplerian part and a time-dependent perturbation. The system is regularized by the application of the Kuustanheimo–Stiefel variables. The composition rule of Laskar and Robutel with a symplectic corrector is applied. The second integrator is based on the approximate, averaged Hamiltonian. Non-canonical Lie–Poisson bracket is applied allowing the use of non-singular vectorial elements. Both methods prove superior when compared to their previously published counterparts.

Key words: methods: analytical – methods: numerical – celestial mechanics – comets: general – Oort Cloud.

1 INTRODUCTION

Galactic tides are one of the essential factors determining the evolution of cometary orbits in the Oort Cloud. In the absence of an analytical solution describing the motion of comets under the action of the complete Galactic tide potential, numerical integration remains the main path to the understanding of the Oort Cloud dynamics between sporadic events like stellar encounters. Gaining knowledge of a dynamical system through numerical integration is a fairly time-consuming process: huge samples of orbits spanning the whole phase space have to be simulated. In recent years, a number of papers were published proposing new tools that may replace a slow, general purpose integrator of high order. Brassier (2001) vaguely reported the application of a presumably fast symplectic integrator of Mikkola. Fast mappings were proposed in Fouchard (2004); Fouchard et al. (2005, 2006), where a detailed accuracy and performance tests can also be found. Another line of improvement was proposed by Breiter & Ratajczak (2005) (see also Breiter & Ratajczak 2006) who suggested the use of non-canonical Hamiltonian formalism. Their Lie–Poisson integrator was designed for axially symmetric Galactic disc perturbations.

In the present paper, we report two complementary integrators that extend and improve the methods presented in Fouchard (2004); Fouchard et al. (2005, 2006) and Breiter & Ratajczak (2005). Both methods belong to a class of Hamiltonian splitting methods: one of them integrates the exact equations of motion, and the other one handles a first-order normalized (averaged) system.

Using the terminology of McLachlan & Quispel (2002), a splitting method consists of three elements: partitioning the right-hand sides into a sum few vector fields, solving the equations of motion induced by each vector field,¹ and combining these solutions to yield an integrator. The last element (to a large extent independent of the first two) is usually referred to as ‘composition’. Thus a splitting method for a particular system necessarily involves some composition method responsible for its local truncation error, but it is the partitioning that determines additional properties of the integrator. Namely, if the system is Hamiltonian and each vector field remains Hamiltonian, the integrator will conserve the symplectic or Poisson structure of the flow regardless of the composition method applied. As a side effect, the Hamiltonian function has no secular error apart from round-off effects.

Sometimes a splitting method can be improved by adding an extra stage known as a corrector. Derived from some combination of the partitioned right-hand side terms, it does not increase the power of step size in the local truncation error estimate, yet it may effectively decrease the local error by introducing an extra factor independent of the step size. For example, the symplectic correctors may diminish the error of a Hamiltonian function in the situation when one of the terms in a partitioned Hamiltonian is much smaller than the other (Wisdom, Holman & Touma 1996; Laskar & Robutel 2001; McLachlan & Quispel 2002). Our first integrator (LARKS – after the names of Laskar, Robutel, Kuustanheimo and Stiefel), described in Section 2, employs the composition method and the symplectic corrector of Laskar & Robutel (2001) in the framework

*E-mail: breiter@amu.edu.pl (SB); fouchard@imcce.fr (MF); astromek@amu.edu.pl (RR); bori@moon.astro.amu.edu.pl (WB)

¹ The solutions can be either exact or approximate, but we assume only the former case in the present paper.

of the Kuustanheimo–Stiefel (KS) variables. To a large extent, it can be considered as a direct descendant of the T-REX method of Breiter (1998).

The second method, presented in Section 3, integrates first-order normalized equations of motion that no longer depend on the mean anomaly. They are derived from a Hamiltonian function with a non-canonical Lie–Poisson bracket. Thanks to the use of ‘vectorial elements’ (dimensionless Laplace vector and angular momentum vector), no singularities are met regardless of orbital eccentricity and inclination. This approach already proved fruitful for the Galactic disc problem (Breiter & Ratajczak 2005, 2006). The method will be referred to as Lie–Poisson with Vectorial elements (LPV). Unlike LARKS, the integrator is based on the partition of the Hamiltonian into three terms of similar magnitude, thus the application of a corrector is neither easy nor advantageous, so only usual symmetric composition methods are applied.

Both integrators are also supplied with algorithms that allow the propagation of the associated variational equations. This feature is of great importance for distinguishing regular and chaotic orbits, because many of the chaos detectors rely on checking the exponential growth of the variations vector.

Section 4 presents performance tests and resolves some technical questions related to the step size choice.

2 REGULARIZED SYMPLECTIC INTEGRATOR

2.1 Equations of motion

2.1.1 Hamiltonian in Cartesian variables

Let us consider the motion of a comet in a right-handed heliocentric reference frame $Oxyz$. The fundamental plane Oxy is parallel to the Galactic disc and the axis Oz points towards the North Galactic Pole. If we fix the orientation of the Ox axis such that at the initial epoch $t = 0$ it is directed to the Galactic Centre, we will obtain an explicitly time-dependent problem of the heliocentric Keplerian motion perturbed by the tidal force of the Galaxy. The time dependence comes from the orbital motion of the Sun around the Galactic Centre. Assuming the circular orbit of the Sun, we can represent the heliocentric motion of the Galactic Centre as a uniform rotation with the angular rate $\Omega_0 < 0$. Thus, similar to Fouchard (2004), we can assume the Hamiltonian function

$$\mathcal{H} = \mathcal{H}_0 + \mathcal{H}_1 \quad (1)$$

$$\mathcal{H}_0 = \frac{1}{2} (X^2 + Y^2 + Z^2) - \frac{\mu}{r}, \quad (2)$$

$$\mathcal{H}_1 = \frac{1}{2} (\mathcal{G}_1 x_1^2 + \mathcal{G}_2 y_1^2 + \mathcal{G}_3 z^2), \quad (3)$$

where x_1 and y_1 are the projections of a comet radius vector $\mathbf{r} = (x, y, z)^T$ on to the direction towards the Galactic Centre and its perpendicular

$$\begin{aligned} x_1 &= x \cos \Omega_0 t + y \sin \Omega_0 t, \\ y_1 &= -x \sin \Omega_0 t + y \cos \Omega_0 t. \end{aligned} \quad (4)$$

The uppercase X, Y and Z stand for the momenta canonically conjugate to the respective lowercase coordinates.

The physical constants appearing in the Hamiltonian involve the heliocentric gravitational parameter $\mu = GM_\odot$ and parameters \mathcal{G}_i related to the Oort constants of our Galaxy. Following Levison,

Dones & Duncan (2001), we adopt

$$\begin{aligned} \mathcal{G}_2 &= -\mathcal{G}_1 = 7.0706 \times 10^{-16} \text{ yr}^{-2}, \\ \mathcal{G}_3 &= 5.6530 \times 10^{-15} \text{ yr}^{-2}, \\ \Omega_0 &= -\sqrt{\mathcal{G}_2}. \end{aligned} \quad (5)$$

Introducing the first of equations (5) explicitly, we can rewrite \mathcal{H}_1 as

$$\mathcal{H}_1(x, y, z, t) = \frac{1}{2} \mathcal{G}_2 [(y^2 - x^2)C - 2xyS] + \frac{1}{2} \mathcal{G}_3 z^2, \quad (6)$$

where

$$C = \cos(2\Omega_0 t), \quad S = \sin(2\Omega_0 t). \quad (7)$$

It is well known that in cometary problems one cannot expect to meet moderate eccentricities of orbits; some kind of regularization will become unavoidable if a fixed step integrator is to be applied. One of the standard regularizing tools, successfully tested in celestial mechanics over decades, is the application of the so-called KS transformation that turns a Kepler problem into a harmonic oscillator at the expense of increasing the number of degrees of freedom (Stiefel & Scheifele 1971). Out of numerous ways of settling the KS variables in the canonical formalism, we choose the approach of Deprit, Elpe & Ferrer (1994), warning readers that the labelling of variables may differ from the one commonly repeated after the Stiefel and Scheifele textbook.

2.1.2 KS variables

Leaving apart the in-depth quaternion interpretation of the KS transformation given by Deprit et al. (1994), we restrict ourselves to providing the basic set of transformation formulae, treating the KS variables as a formal column vector. In the phase space of the KS coordinates, $\mathbf{u} = (u_0, u_1, u_2, u_3)^T$ and KS momenta $\mathbf{U} = (U_0, U_1, U_2, U_3)^T$, the former are defined by means of the inverse transformation

$$\begin{aligned} x &= (u_0^2 + u_1^2 - u_2^2 - u_3^2)/\alpha, \\ y &= 2(u_1 u_2 + u_0 u_3)/\alpha, \\ z &= 2(u_1 u_3 - u_0 u_2)/\alpha, \end{aligned} \quad (8)$$

where α is an arbitrary parameter with a dimension of length. A dimension raising transformation cannot be bijective, so the inverse of (8) is to some extent arbitrary. Following Deprit et al. (1994), we adopt

$$\mathbf{u} = \sqrt{\frac{\alpha}{2(r+x)}} (0, r+x, y, z)^T, \quad (9)$$

for $x \geq 0$, and

$$\mathbf{u} = \sqrt{\frac{\alpha}{2(r-x)}} (-z, y, r-x, 0)^T, \quad (10)$$

otherwise. A remarkable property of this transformation is that the distance r becomes a quadratic function of u_i , namely

$$r = \sqrt{x^2 + y^2 + z^2} = \frac{u_0^2 + u_1^2 + u_2^2 + u_3^2}{\alpha} = \frac{\mathbf{u}^2}{\alpha}. \quad (11)$$

The momenta conjugate to \mathbf{u} are defined as

$$\mathbf{U} = \frac{2}{\alpha} \begin{pmatrix} u_0 X + u_3 Y - u_2 Z \\ u_1 X + u_2 Y + u_3 Z \\ -u_2 X + u_1 Y - u_0 Z \\ -u_3 X + u_0 Y + u_1 Z \end{pmatrix}. \quad (12)$$

The inverse transformation, allowing the computation of $\mathbf{R} = (X, Y, Z)^T$,

$$\mathbf{R} = \frac{1}{2r} \begin{pmatrix} u_0 U_0 + u_1 U_1 - u_2 U_2 - u_3 U_3 \\ u_3 U_0 + u_2 U_1 + u_1 U_2 + u_0 U_3 \\ -u_2 U_0 + u_3 U_1 - u_0 U_2 + u_1 U_3 \end{pmatrix}, \quad (13)$$

can be supplemented with the identity

$$u_1 U_0 - u_0 U_1 - u_3 U_2 + u_2 U_3 = 0, \quad (14)$$

that may serve as one of the accuracy tests during numerical integration.

In order to achieve the regularization without leaving the canonical formalism, we have to change the independent variable from t to a fictitious time s and consider the extended phase space of dimension 10, with a new pair of conjugate variables (u^* , U^*). Thus in the extended set of canonical KS variables, the motion of a comet is governed by the Hamiltonian function

$$\mathcal{M} = \frac{4\mathbf{u}^2}{\alpha^2} (\mathcal{K}_0 + U^* + \mathcal{K}_1) = 0, \quad (15)$$

where \mathcal{K}_0 and \mathcal{K}_1 stand for \mathcal{H}_0 and \mathcal{H}_1 , respectively, expressed in terms of the extended KS variables set. The presented transformation is univalent, hence the respective Hamiltonians will have different functional forms, but equal values: $\mathcal{H}_0 = \mathcal{K}_0$, $\mathcal{H}_1 = \mathcal{K}_1$. Restricting the motion to the manifold of $\mathcal{M} = 0$ is of fundamental importance to the canonical change of independent variable; in practical terms we achieve it by setting

$$U^* = -\mathcal{K}_0 - \mathcal{K}_1, \quad (16)$$

at the beginning of the numerical integration.²

Splitting the Hamiltonian function \mathcal{M} into a sum of the principal term \mathcal{M}_0 and a perturbation \mathcal{M}_1 , we have

$$\mathcal{M}_0 = \frac{1}{2} U^2 + (4U^*/\alpha^2) \mathbf{u}^2, \quad (17)$$

$$\mathcal{M}_1 = \frac{4\mathbf{u}^2}{\alpha^2} \mathcal{H}_1(x, y, z, t). \quad (18)$$

We find it convenient to maintain \mathcal{H}_1 as a function of Cartesian coordinates and time, because the values of x , y , z can be quickly computed from equations (8) and partial derivatives required in next sections are simple enough to provide compact expressions:

$$\left(\frac{\partial \mathbf{r}}{\partial \mathbf{u}} \right)^T = \frac{2}{\alpha} \begin{pmatrix} u_0 & u_3 & -u_2 \\ u_1 & u_2 & u_3 \\ -u_2 & u_1 & -u_0 \\ -u_3 & u_0 & u_1 \end{pmatrix}. \quad (19)$$

Although nothing prohibits u^* and t to differ by an additive constant, we do not profit from this freedom and so we will use the symbol t in most of instances instead of the formal u^* . In the next section, we provide equations of motion generated by \mathcal{M}_0 and \mathcal{M}_1 alone; the complete equations of motion can quickly be obtained by adding the respective right-hand sides.

² More details concerning this kind of Hamiltonian regularization can be found in Szebehely (1967), Stiefel & Scheifele (1971) and Mikkola & Wiegert (2002).

2.2 Canonical splitting method

2.2.1 Keplerian motion

The principal virtue of the KS variables consists in their ability of transforming the Kepler problem into a harmonic oscillator. Indeed, \mathcal{M}_0 leads to the equations of motion

$$\frac{d\mathbf{u}}{ds} = \frac{\partial \mathcal{M}_0}{\partial \mathbf{U}} = \mathbf{U}, \quad (20)$$

$$\frac{d\mathbf{U}}{ds} = -\frac{\partial \mathcal{M}_0}{\partial \mathbf{u}} = -(8U^*/\alpha^2) \mathbf{u}, \quad (21)$$

$$\frac{dt}{ds} = \frac{\partial \mathcal{M}_0}{\partial U^*} = 4\mathbf{u}^2/\alpha^2, \quad (22)$$

$$\frac{dU^*}{ds} = -\frac{\partial \mathcal{M}_0}{\partial t} = 0. \quad (23)$$

Equations (20) and (21) define a four-dimensional oscillator with a frequency

$$\omega = 2 \frac{\sqrt{2U^*}}{\alpha}, \quad (24)$$

and equation (23) indicates that the frequency is constant. Equation (22) explains the meaning of the fictitious time s : we can rewrite it as

$$\frac{ds}{dt} = \frac{\alpha}{4r}. \quad (25)$$

Thus, supposing that we study Keplerian motion on an ellipse with a semi-axis a , ds/dt equals to $(\alpha/4a)dE/d\ell$, where E and ℓ are the eccentric and the mean anomaly, respectively. It means that apart from a multiplier, the fictitious time s behaves like eccentric anomaly, albeit the former is not an angle and cannot be treated 'modulo period'. Thanks to the introduction of α , the fictitious time s has the dimension of time and if we assume

$$\alpha = \frac{2\mu}{|U^*|}, \quad (26)$$

orbital periods in s and t will be equal in the elliptic motion. It should be noted, however, that the oscillator defined by \mathcal{M}_0 has the frequency $\omega = n/2$ (where n is the mean motion), i.e. the Keplerian ellipse period in Cartesian coordinates is two times shorter than the KS oscillator's period in t . This fact is a direct consequence of equations (8); by a simple analogy, the square of a 2π periodic sine function is only π periodic. Thus, selecting the integration step, one has to bear in mind that one cycle of the KS oscillator maps on two revolutions in the Cartesian space.

For $U^* > 0$, the map Φ_0 representing the solution of equations (20)–(23) can be directly quoted from Breiter (1998). If Δ is the fictitious time-step, then

$$\Phi_{0,\Delta} : \begin{pmatrix} \mathbf{u} \\ \mathbf{U} \\ U^* \end{pmatrix} \rightarrow \begin{pmatrix} \mathbf{u} \cos \omega \Delta + \mathbf{U} \omega^{-1} \sin \omega \Delta \\ -\mathbf{u} \omega \sin \omega \Delta + \mathbf{U} \cos \omega \Delta \\ U^* \end{pmatrix}. \quad (27)$$

Additionally, if $\mathbf{v} = \Phi_{0,\Delta} \mathbf{u}$ and $\mathbf{V} = \Phi_{0,\Delta} \mathbf{U}$ are the final values of variables,

$$\Phi_{0,\Delta} : t \rightarrow t + \frac{2\Delta}{\alpha^2} \left(\mathbf{u}^2 + \frac{\mathbf{U}^2}{\omega^2} \right) + 2 \frac{\mathbf{u}^T \mathbf{U} - \mathbf{v}^T \mathbf{V}}{\alpha^2 \omega^2}. \quad (28)$$

One may easily check that the sum $\mathbf{u}^2 + \mathbf{U}^2 \omega^{-2}$ is invariant under Φ_0 and it can be replaced by $\mathbf{v}^2 + \mathbf{V}^2 \omega^{-2}$ in practical computations of the Kepler equation (28).

It may happen, however, that $U^* < 0$ and the motion is (at least temporarily) hyperbolic. A simple modification of Φ_0 in that case amounts to taking

$$\omega = 2 \frac{\sqrt{-2U^*}}{\alpha}, \quad (29)$$

and replacing equations (27) and (28) by

$$\Phi_{0,\Delta} : \begin{pmatrix} \mathbf{u} \\ \mathbf{U} \\ U^* \end{pmatrix} \rightarrow \begin{pmatrix} \mathbf{u} \cosh \omega \Delta + \mathbf{U} \omega^{-1} \sinh \omega \Delta \\ \mathbf{u} \omega \sinh \omega \Delta + \mathbf{U} \cosh \omega \Delta \\ U^* \end{pmatrix}, \quad (30)$$

and

$$\Phi_{0,\Delta} : t \rightarrow t + \frac{2\Delta}{\alpha^2} \left(\mathbf{u}^2 - \frac{\mathbf{U}^2}{\omega^2} \right) - 2 \frac{\mathbf{u}^T \mathbf{U} - \mathbf{v}^T \mathbf{V}}{\alpha^2 \omega^2}. \quad (31)$$

Similarly to the elliptic case, $\mathbf{u}^2 - \mathbf{U}^2/\omega^2$ is invariant under Φ_0 .

We do not provide the complete formulation for $U^* = 0$, because the probability of meeting this case is practically negligible. Actually, using the SBAB or SBABC composition methods (see Section 2.4), it is even not easy to create this case intentionally. We only observe that for a parabolic motion the selection rule of α obviously cannot be based on U^* and then any choice, like α equal to the osculating perihelion distance, is acceptable. The parabolic solution is easily derivable from equations (20)–(23) that lead to constant \mathbf{U} , linear functions of s for \mathbf{u} and the quadratic function of s for t , when $U^* = 0$.

2.2.2 Galactic tide

Hamiltonian \mathcal{M}_1 has a nice property of being independent on momenta. Thus a half of the equations of motion have right-hand sides equal to zero, and the remaining right-hand sides are constant:

$$\frac{d\mathbf{u}}{ds} = \frac{\partial \mathcal{M}_1}{\partial \mathbf{U}} = \mathbf{0}, \quad (32)$$

$$\frac{dt}{ds} = \frac{\partial \mathcal{M}_1}{\partial U^*} = 0, \quad (33)$$

$$\frac{d\mathbf{U}}{ds} = -\frac{\partial \mathcal{M}_1}{\partial \mathbf{u}} = -\mathbf{F}(\mathbf{u}, t), \quad (34)$$

$$\frac{dU^*}{ds} = -\frac{\partial \mathcal{M}_1}{\partial t} = -\frac{4\mathbf{u}^2}{\alpha^2} \frac{\partial \mathcal{H}_1}{\partial t} = -F^*(\mathbf{u}, t). \quad (35)$$

Accordingly, all KS coordinates are constant, the physical time t does not flow, and the momenta are subjected to a linear ‘kick’

$$\Phi_{1,\Delta} : \begin{pmatrix} \mathbf{u} \\ t \\ \mathbf{U} \\ U^* \end{pmatrix} \rightarrow \begin{pmatrix} \mathbf{u} \\ t \\ \mathbf{U} - \Delta \mathbf{F}(\mathbf{u}, t) \\ U^* - \Delta F^*(\mathbf{u}, t) \end{pmatrix}. \quad (36)$$

Mixing Cartesian and KS variables for the sake of brevity, we can represent \mathbf{F} and F^* as

$$\mathbf{F} = \frac{8\mathcal{H}_1}{\alpha^2} \mathbf{u} + \frac{4\mathbf{u}^2}{\alpha^2} \frac{\partial \mathcal{H}_1}{\partial \mathbf{u}} \quad (37)$$

$$F^* = \frac{4\mathbf{u}^2}{\alpha^2} \Omega_0 \mathcal{G}_2 \xi_3, \quad (38)$$

where

$$\begin{aligned} \frac{\partial \mathcal{H}_1}{\partial \mathbf{u}} &= -\mathcal{G}_2 \xi_2 \frac{\partial x}{\partial \mathbf{u}} + \mathcal{G}_2 \xi_1 \frac{\partial y}{\partial \mathbf{u}} + \mathcal{G}_3 z \frac{\partial z}{\partial \mathbf{u}} \\ \xi_1 &= yC - xS, \end{aligned} \quad (39)$$

$$\xi_2 = xC + yS, \quad (40)$$

$$\xi_3 = (x^2 - y^2)S - 2xyC,$$

$\partial x/\partial \mathbf{u}$ is the first column of the Jacobian matrix (19), and so on.

2.2.3 Symplectic corrector

One of the advantages offered by Laskar & Robutel (2001) integrators is a simple definition of a symplectic corrector – an extra stage that improves the accuracy in perturbed motion problems. The symplectic corrector is defined as a solution of equations of motion generated by

$$\mathcal{M}_c = \{ \{ \mathcal{M}_0, \mathcal{M}_1 \}, \mathcal{M}_1 \}, \quad (41)$$

where $\{, \}$ is the canonical (or ‘symplectic’) Poisson bracket in the phase space spanned by $\mathbf{u}, t, \mathbf{U}, U^*$. Observing that \mathcal{M}_0 is quadratic in \mathbf{U} and linear in U^* , we easily obtain

$$\mathcal{M}_c(\mathbf{u}, t) = \sum_{i=0}^3 \left(\frac{\partial \mathcal{M}_1}{\partial u_i} \right)^2 = F^2. \quad (42)$$

The general form of equations of motion derived from \mathcal{M}_c is simple

$$\frac{d\mathbf{u}}{ds} = \frac{\partial \mathcal{M}_c}{\partial \mathbf{U}} = \mathbf{0}, \quad (43)$$

$$\frac{dt}{ds} = \frac{\partial \mathcal{M}_c}{\partial U^*} = 0, \quad (44)$$

$$\frac{dU_j}{ds} = -\frac{\partial \mathcal{M}_c}{\partial u_j} = -2 \left(\frac{\partial \mathbf{F}}{\partial u_j} \right) \cdot \mathbf{F}(\mathbf{u}, t), \quad (45)$$

$$\frac{dU^*}{ds} = -\frac{\partial \mathcal{M}_c}{\partial t} = -2 \left(\frac{\partial \mathbf{F}}{\partial t} \right) \cdot \mathbf{F}(\mathbf{u}, t), \quad (46)$$

and their solution is elementary, resulting in

$$\Phi_{c,\Delta} : \begin{pmatrix} \mathbf{u} \\ t \\ U_j \\ U^* \end{pmatrix} \rightarrow \begin{pmatrix} \mathbf{u} \\ t \\ U_j - 2\Delta \left(\frac{\partial \mathbf{F}}{\partial u_j} \right) \cdot \mathbf{F} \\ U^* - 2\Delta \left(\frac{\partial \mathbf{F}}{\partial t} \right) \cdot \mathbf{F} \end{pmatrix}. \quad (47)$$

In spite of a formally simple form, equations (47) involve rather complicated expressions for the second derivatives of \mathcal{M}_1 , because

$$\frac{\partial \mathbf{F}}{\partial u_j} \cdot \mathbf{F}(\mathbf{u}, t) = \sum_{i=0}^3 \frac{\partial^2 \mathcal{M}_1}{\partial u_i \partial u_j} \frac{\partial \mathcal{M}_1}{\partial u_i}, \quad (48)$$

$$\frac{\partial \mathbf{F}}{\partial t} \cdot \mathbf{F}(\mathbf{u}, t) = \sum_{i=0}^3 \frac{\partial^2 \mathcal{M}_1}{\partial u_i \partial t} \frac{\partial \mathcal{M}_1}{\partial u_i}. \quad (49)$$

The Hessian matrix of \mathcal{M}_1 can be represented as a sum

$$\frac{\partial^2 \mathcal{M}_1}{\partial \mathbf{u}^2} = \frac{8}{\alpha^2} \left[\mathcal{H}_1 \mathbf{I}_4 + \mathbf{u} \left(\frac{\partial \mathcal{H}_1}{\partial \mathbf{u}} \right)^T + \frac{\partial \mathcal{H}_1}{\partial \mathbf{u}} \mathbf{u}^T + \frac{u^2}{2} \frac{\partial^2 \mathcal{H}_1}{\partial u^2} \right], \quad (50)$$

where \mathbf{I}_4 is a 4×4 unit matrix, and $\mathbf{x}\mathbf{y}^T$ stands for the tensor product with components $[\mathbf{x}\mathbf{y}^T]_{ij} = x_i y_j$. The Hessian of \mathcal{H}_1 is composed of two matrices

$$\frac{\partial^2 \mathcal{H}_1}{\partial \mathbf{u}^2} = \frac{2}{\alpha} (\mathbf{G} + \mathbf{A}). \quad (51)$$

The matrix \mathbf{G} is

$$\mathbf{G} = \begin{pmatrix} -\mathcal{G}_2 \xi_2 & 0 & -\mathcal{G}_3 z & \mathcal{G}_2 \xi_1 \\ 0 & -\mathcal{G}_2 \xi_2 & \mathcal{G}_2 \xi_1 & \mathcal{G}_3 z \\ -\mathcal{G}_3 z & \mathcal{G}_2 \xi_1 & \mathcal{G}_2 \xi_2 & 0 \\ \mathcal{G}_2 \xi_1 & \mathcal{G}_3 z & 0 & \mathcal{G}_2 \xi_2 \end{pmatrix}. \quad (52)$$

The matrix \mathbf{A} is symmetric, so only 10 of its elements have to be specified; using explicitly the KS coordinates, we obtain

$$\begin{aligned} a_{11} &= \mathcal{G}_3 u_2^2 - \mathcal{G}_2 [(u_0^2 - u_3^2) C + 2 u_0 u_3 S], \\ a_{22} &= \mathcal{G}_3 u_3^2 - \mathcal{G}_2 [(u_1^2 - u_2^2) C + 2 u_1 u_2 S], \\ a_{33} &= \mathcal{G}_3 u_0^2 + \mathcal{G}_2 [(u_1^2 - u_2^2) C + 2 u_1 u_2 S], \\ a_{44} &= \mathcal{G}_3 u_1^2 + \mathcal{G}_2 [(u_0^2 - u_3^2) C + 2 u_0 u_3 S], \\ a_{12} &= -\mathcal{G}_3 u_2 u_3 \\ &\quad - \mathcal{G}_2 [(u_0 u_1 - u_2 u_3) C + (u_0 u_2 + u_1 u_3) S], \\ a_{13} &= \mathcal{G}_3 u_0 u_2 \\ &\quad + \mathcal{G}_2 [(u_0 u_2 + u_1 u_3) C - (u_0 u_1 - u_2 u_3) S], \\ a_{14} &= -\mathcal{G}_3 u_1 u_2 + \mathcal{G}_2 [2 u_0 u_3 C - (u_0^2 - u_3^2) S], \\ a_{23} &= -\mathcal{G}_3 u_0 u_3 + \mathcal{G}_2 [2 u_1 u_2 C - (u_1^2 - u_2^2) S], \\ a_{24} &= \mathcal{G}_3 u_1 u_3 \\ &\quad + \mathcal{G}_2 [(u_0 u_2 + u_1 u_3) C - (u_0 u_1 - u_2 u_3) S], \\ a_{34} &= -\mathcal{G}_3 u_0 u_1 \\ &\quad + \mathcal{G}_2 [(u_0 u_1 - u_2 u_3) C + (u_0 u_2 + u_1 u_3) S]. \end{aligned} \quad (53)$$

Partial derivatives required in (49) are simpler:

$$\frac{\partial^2 \mathcal{M}_1}{\partial \mathbf{u} \partial t} = \frac{8 \Omega_0 \mathcal{G}_2}{\alpha^2} (\xi_3 \mathbf{u} - u^2 \mathbf{H}), \quad (54)$$

where

$$\mathbf{H} = \begin{pmatrix} (u_3 x + u_0 y) C + (u_3 y - u_0 x) S \\ (u_2 x + u_1 y) C + (u_2 y - u_1 x) S \\ (u_1 x - u_2 y) C + (u_1 y + u_2 x) S \\ (u_0 x - u_3 y) C + (u_0 y + u_3 x) S \end{pmatrix}. \quad (55)$$

At the first glimpse, one may hesitate if the cost of computing the corrector is worth the gain in accuracy from the point of view of the computation time. The doubts, however, will be quickly dismissed when the tangent map is to be attached to the integrator. The next section shows that the second derivatives presented above are also required for the tangent map, hence in that case the corrector is actually evaluated almost at no cost.

2.3 Tangent maps

Considering the sensitivity of motion to the initial conditions, either for the chaos test or for the differential correction of orbits, one has to know the evolution of the tangent vector δ describing an infinitesimal displacement with respect to the fiducial trajectory in the phase space. Although δ is formally infinitesimal, it obeys homogeneous linear equations of motion (variational equations), which means that we can multiply it by an arbitrary constant and use the initial value of δ normalized to $\delta = 1$. From the formal point of view, we should integrate the linear system of variational equations derived from the equations of motion generated by \mathcal{M} ; but this is by no means a simple way – far more complicated than taking the shortcut indicated by Mikkola & Innanen (1999) that amounts to linearizing the maps Φ_0 and Φ_1 . Thus we provide expressions of ‘tangent maps’ $D\Phi_0$ and $D\Phi_1$ that serve to propagate the tangent vector δ simultaneously with the integration of \mathbf{u} , \mathbf{U} , t and U^* . As a matter of fact, we should also provide a tangent map $D\Phi_c$, but computing third derivatives of \mathcal{M} does not seem attractive and we cut the Gordian knot by neglecting the corrector’s influence on δ .

2.3.1 Keplerian tangent map

Differentiating equations (27), (28) and their hyperbolic counterparts, we obtain the tangent map $D\Phi_0$ as the propagation rules for the tangent vector δ . The initial values of δ will be labelled $\delta \mathbf{u}$, $\delta \mathbf{U}$, δt and δU^* ; the values after the fictitious time-step Δ will be referred to as $\delta \mathbf{v}$, $\delta \mathbf{V}$, $\delta t'$ and δV^* . Thus $\delta V^* = \delta U^*$, and

$$\delta \mathbf{v} = (\delta \mathbf{u}) c_* + (\delta \mathbf{U}) \frac{s_*}{\omega} + \frac{(\delta \omega)}{\omega} \left(\mathbf{V} \Delta - \mathbf{U} \frac{s_*}{\omega} \right), \quad (56)$$

$$\delta \mathbf{V} = \mp (\delta \mathbf{u}) \omega s_* + (\delta \mathbf{U}) c_* \mp (\delta \omega) (\omega \mathbf{v} \Delta + \mathbf{u} s_*), \quad (57)$$

$$\begin{aligned} \delta t' &= (\delta t) + \frac{4 \Delta}{\alpha^2} \left[\mathbf{u} \cdot (\delta \mathbf{u}) \pm \frac{\mathbf{U} \cdot (\delta \mathbf{U})}{\omega^2} \mp \frac{(\delta \omega)}{\omega^3} U^2 \right] \\ &\quad \pm \frac{2}{\alpha^2 \omega^2} [(\delta \mathbf{u}) \cdot \mathbf{U} + \mathbf{u} \cdot (\delta \mathbf{U}) - (\delta \mathbf{v}) \cdot \mathbf{V} - \mathbf{v} \cdot (\delta \mathbf{V})] \\ &\quad \mp \frac{4(\delta \omega)}{\alpha^2 \omega^3} (\mathbf{u} \cdot \mathbf{U} - \mathbf{v} \cdot \mathbf{V}), \end{aligned} \quad (58)$$

$$\delta \omega = \pm \frac{4(\delta U^*)}{\alpha^2 \omega}. \quad (59)$$

If $U^* > 0$, the upper signs should be taken in the above equations and $s_* = \sin \omega \Delta$, $c_* = \cos \omega \Delta$. In the opposite case, $s_* = \sinh \omega \Delta$, $c_* = \cosh \omega \Delta$, and the lower signs are to be adopted.

2.3.2 Tidal tangent map

Differentiating the galactic tide map (36), we obtain formally simple expressions of the tangent map $D\Phi_1$

$$D\Phi_{1,\Delta} : \begin{pmatrix} \delta \mathbf{u} \\ \delta t \\ \delta \mathbf{U} \\ \delta U^* \end{pmatrix} \rightarrow \begin{pmatrix} \delta \mathbf{u} \\ \delta t \\ \delta \mathbf{U} - \Delta \mathbf{P} \\ \delta U^* - \Delta P^* \end{pmatrix}, \quad (60)$$

where

$$\begin{aligned} \mathbf{P} &= \left[\frac{\partial \mathbf{F}}{\partial \mathbf{u}} \right] (\delta \mathbf{u}) + (\delta t) \frac{\partial \mathbf{F}}{\partial t} \\ &= \left[\frac{\partial^2 \mathcal{M}_1}{\partial \mathbf{u}^2} \right] (\delta \mathbf{u}) + (\delta t) \left[\frac{\partial^2 \mathcal{M}_1}{\partial \mathbf{u} \partial t} \right], \end{aligned} \quad (61)$$

$$\begin{aligned} \mathbf{P}^* &= \left[\frac{\partial \mathbf{F}^*}{\partial \mathbf{u}} \right] (\delta \mathbf{u}) + (\delta t) \frac{\partial \mathbf{F}^*}{\partial t} \\ &= \frac{\partial^2 \mathcal{M}_1}{\partial \mathbf{u} \partial t} (\delta \mathbf{u}) + (\delta t) \frac{\partial^2 \mathcal{M}_1}{\partial t^2}. \end{aligned} \quad (62)$$

Most of the derivatives required for this tangent map can be found in Section 2.2.3, except for

$$\frac{\partial^2 \mathcal{M}_1}{\partial t^2} = \frac{8r}{\alpha} \mathcal{G}_2 \Omega_0^2 [(x^2 - y^2)C + 2xyS]. \quad (63)$$

2.3.3 Initial conditions for the tangent map

Choosing an appropriate initial direction of the variation vector is important; most of all, one should avoid the direction of δ parallel to the right-hand sides of equations of motion, because it leads to underestimated values of the maximum Lyapunov exponent and related chaos indicators (Barrio 2005). An optimum choice of initial δ is orthogonal to the flow. For the LARKS integrator, we have adopted a simplified approach, setting the variations orthogonal to the Keplerian flow, i.e.

$$\begin{aligned} \delta \mathbf{u} &= -\mathbf{U}' = 8\alpha^{-2} \mathbf{U}^* \mathbf{u}, \\ \delta \mathbf{U} &= \mathbf{u}' = \mathbf{U}, \\ \delta t &= -(U^*)' = 0, \\ \delta U^* &= t' = 4\alpha^{-2} \mathbf{u}^2. \end{aligned} \quad (64)$$

2.4 Laskar–Robutel integrators

The composition methods of Laskar & Robutel (2001) differ from usual recipes, because regardless of the number of ‘stages’ involved in one step, they all remain second-order integrators according to the formal estimates (in this context the term ‘high order’ used by Laskar and Robutel is a bit misleading). However, if the Hamiltonian has been split into a leading term and a perturbation having a small parameter ε as a factor, the truncation error of the integrator is $\max(\varepsilon^2 h^3, \varepsilon h^m)$ where m is the number of stages involved in one step. The second term of this sum is similar to classical composition methods errors, and the first can be quite small for weakly perturbed problems. At the expense of the $\varepsilon^2 h^3$ term in the error estimate, the authors were able to avoid backward stages that degrade numerical properties of usual composition methods. The use of a corrector improves the integrator by reducing the truncation error: its first term drops to $\varepsilon^2 h^5$. Following the recommendation of Laskar & Robutel (2001), we have adopted their SBABC3 method as the optimum choice. In this case a single step of LARKS with the step size h can be written as

$$\begin{aligned} \Phi_h &= \Phi_{c,q} \circ \Phi_{1,d_1} \circ \Phi_{0,c_2} \circ \Phi_{1,d_2} \circ \Phi_{0,c_3} \circ \\ &\quad \circ \Phi_{1,d_2} \circ \Phi_{0,c_2} \circ \Phi_{1,d_1} \circ \Phi_{c,q}, \end{aligned} \quad (65)$$

where

$$\begin{aligned} d_1 &= h/12, & d_2 &= (5/12)h, \\ c_2 &= (1/2 - \sqrt{5}/10)h, & c_3 &= h/\sqrt{5}, \\ q &= -h^3(13 - 5\sqrt{5})/288. \end{aligned} \quad (66)$$

However, this choice has not been made without numerical tests involving other composition rules with and without correctors. The results of our tests are given in Section 4.

The tangent map $D\Phi_h$ is constructed similarly, but we have decided to skip the correction part. There is no need to struggle for a high accuracy of variations vector as far as we are interested only in detecting its exponential growth. Thus

$$\begin{aligned} D\Phi_h &= D\Phi_{1,d_1} \circ D\Phi_{0,c_2} \circ D\Phi_{1,d_2} \circ D\Phi_{0,c_3} \circ \\ &\quad \circ D\Phi_{1,d_2} \circ D\Phi_{0,c_2} \circ D\Phi_{1,d_1}. \end{aligned} \quad (67)$$

3 LIE-POISSON INTEGRATOR FOR THE AVERAGED SYSTEM

3.1 Equations of motion

The integrator presented in the previous section solves the equations of motion in the fixed reference frame, where the radial component of the Galactic tide is explicitly time-dependent. Our second method can be more conveniently discussed in a rotating heliocentric reference frame Ox_1y_1z . The Ox_1y_1 plane remains parallel to the Galactic disc, but this time Ox_1 axis is directed towards the Galactic Centre hence the frame rotates around the Oz axis with the angular rate Ω_0 . If we assume the right-handed Ox_1y_1z system of axes and the axis Oz remains directed towards the North Galactic Pole, the rotation is clockwise, which implies $\Omega_0 < 0$. The Hamiltonian function for a comet subjected to the Galactic tide in the rotating frame is given by

$$\mathcal{H} = \mathcal{H}_0 + \mathcal{H}_1, \quad (68)$$

$$\mathcal{H}_0 = \frac{1}{2} (X_1^2 + Y_1^2 + Z^2) - \frac{\mu}{(x_1^2 + y_1^2 + z^2)^{\frac{1}{2}}}, \quad (69)$$

$$\mathcal{H}_1 = \Omega_0 (y_1 X_1 - x_1 Y_1) + \frac{1}{2} (\mathcal{G}_2 (y_1^2 - x_1^2) + \mathcal{G}_3 z^2). \quad (70)$$

The first-order normalization of \mathcal{H} with respect to \mathcal{H}_0 is equivalent to averaging with respect to the mean anomaly ℓ and leads to the new Hamiltonian

$$\mathcal{H}^* = \mathcal{H}_0^* + \mathcal{H}_1^*, \quad (71)$$

$$\mathcal{H}_0^* = -\frac{\mu}{2a}, \quad (72)$$

$$\mathcal{H}_1^* = \frac{1}{2\pi} \int_0^{2\pi} \mathcal{H}_1 d\ell, \quad (73)$$

where the elliptic Keplerian motion is assumed to evaluate the quadrature in (73). The averaged Hamiltonian \mathcal{H}_1^* attains the simplest form if expressed in terms of the Laplace vector \mathbf{e} and a scaled

angular momentum vector \mathbf{h} . Their components are related to the Keplerian orbit elements

$$\mathbf{e} \equiv \begin{pmatrix} e_1 \\ e_2 \\ e_3 \end{pmatrix} = e \begin{pmatrix} \cos \omega \cos \Omega - c \sin \omega \sin \Omega \\ \cos \omega \sin \Omega + c \sin \omega \cos \Omega \\ s \sin \omega \end{pmatrix}, \quad (74)$$

$$\mathbf{h} \equiv \begin{pmatrix} h_1 \\ h_2 \\ h_3 \end{pmatrix} = \sqrt{1 - e^2} \begin{pmatrix} s \sin \Omega \\ -s \cos \Omega \\ c \end{pmatrix}, \quad (75)$$

where e is the eccentricity, $s = \sin I$, $c = \cos I$ are the sine and cosine of the inclination, ω is the argument of perihelion and Ω stands for the longitude of the ascending node with respect to the Galactic Centre. Recalling that in the rotating frame momenta X_1 and Y_1 are not equal to velocities \dot{x}_1 and \dot{y}_1 (the fact that can be immediately deduced from the canonical equations $\dot{x}_1 = \partial \mathcal{H} / \partial X_1$ and $\dot{y}_1 = \partial \mathcal{H} / \partial Y_1$), we assume that the usual transformation rules between Keplerian elements and position/velocity are used with the velocities directly substituted by the momenta. With this approach the Keplerian motion in the rotating frame is described by means of orbital elements that are all constant except for Ω which reflects the frame rotation ($\dot{\Omega} = -\Omega_0$).

Using the ‘vectorial elements’ \mathbf{h} and \mathbf{e} , and letting n to stand for

$$n = \sqrt{\frac{\mu}{a^3}}, \quad (76)$$

we obtain [Correction added after online publication 2007 April 13: in the first line of equation (77), a redundant pair of right square brackets appeared after $\frac{1}{4}$ and have been removed.]

$$\mathcal{H}^* = -\Omega_0 n a^2 h_3 + \frac{1}{4} a^2 [\mathcal{G}_2 (5 e_2^2 - 5 e_1^2 - h_2^2 + h_1^2) + \mathcal{G}_3 (1 - e^2 + 5 e_3^2 - h_3^2)]. \quad (77)$$

Strictly speaking, the Hamiltonian \mathcal{H}^* generates the motion of the mean variables in the linear approximation. Thus, using the solution generated by \mathcal{H}^* we neglect short-period perturbations depending on ℓ that are proportional to the small parameter $\epsilon \approx \mathcal{H}_1 / \mathcal{H}_0$, and we commit an error of the order of ϵ^2 in the evolution of the mean elements. The influence of this approximation will be discussed later; meanwhile we accept the first-order correct, mean elements that liberate us from discussing the mean anomaly ℓ and lead to the constant value of the mean semimajor axis a . As a consequence, we can drop constant terms from \mathcal{H}^* and change the independent variable from time t to τ_1 , such that

$$\frac{d\tau_1}{dt} = \frac{\mathcal{G}_3}{n}. \quad (78)$$

Using the usual approximation $\Omega_0 = -\sqrt{\mathcal{G}_2}$, we introduce a dimensionless parameter

$$\nu = \frac{\Omega_0^2}{\mathcal{G}_3} = \frac{\mathcal{G}_2}{\mathcal{G}_3}, \quad (79)$$

and thus we replace \mathcal{H}^* by [Correction added after online publication 2007 April 13: in the first line of equation (80), $h_1^2 +$ was omitted after the first $\frac{1}{4}$ and an extra $+$ symbol appeared at the end of the line.]

$$\mathcal{H}^* = n a^2 \left[\frac{5}{4} e_3^2 + \frac{1}{4} h_1^2 + \frac{1}{4} h_2^2 + \nu \left(-\frac{5}{4} e_1^2 + \frac{5}{4} e_2^2 + \frac{1}{4} h_1^2 - \frac{1}{4} h_2^2 - n \Omega_0^{-1} h_3 \right) \right]. \quad (80)$$

The vectorial elements can be used to create a Lie–Poisson bracket

$$(f; g) \equiv \left(\frac{\partial f}{\partial \mathbf{v}} \right)^T \mathbf{J}(\mathbf{v}) \frac{\partial g}{\partial \mathbf{v}}, \quad (81)$$

with the structure matrix

$$\mathbf{J}(\mathbf{v}) = \begin{pmatrix} \hat{h} & \hat{e} \\ \hat{e} & \hat{h} \end{pmatrix}. \quad (82)$$

The ‘hat map’ of any vector $\mathbf{x} = (x_1, x_2, x_3)^T$ is defined as

$$\hat{x} = \begin{pmatrix} 0 & -x_3 & x_2 \\ x_3 & 0 & -x_1 \\ -x_2 & x_1 & 0 \end{pmatrix}. \quad (83)$$

This matrix is known as the vector product matrix, because

$$\hat{x} \mathbf{y} = \mathbf{x} \times \mathbf{y}. \quad (84)$$

Using the Lie–Poisson bracket (81), we can write equations of motion for the vectorial elements

$$\mathbf{v} = (h_1, h_2, h_3, e_1, e_2, e_3)^T, \quad (85)$$

in the non-canonical Hamiltonian form

$$\mathbf{v}' = (\mathbf{v}; \mathcal{K}), \quad (86)$$

where derivatives with respect to τ_1 are marked by the ‘prime’ symbol and the scaled Hamiltonian

$$\mathcal{K} = -\frac{\mathcal{H}^*}{n a^2}. \quad (87)$$

Writing equations (86) explicitly, we obtain

$$h_1' = -\frac{5}{2} (1 - \nu) e_2 e_3 + \frac{1 - \nu}{2} h_2 h_3 + \frac{n \nu}{\Omega_0} h_2, \quad (88)$$

$$h_2' = \frac{5}{2} (1 + \nu) e_1 e_3 - \frac{1 + \nu}{2} h_1 h_3 - \frac{n \nu}{\Omega_0} h_1, \quad (89)$$

$$h_3' = \nu (h_1 h_2 - 5 e_1 e_2), \quad (90)$$

$$e_1' = -\frac{4 + \nu}{2} h_2 e_3 + \frac{5}{2} \nu h_3 e_2 + \frac{n \nu}{\Omega_0} e_2, \quad (91)$$

$$e_2' = \frac{4 - \nu}{2} h_1 e_3 + \frac{5}{2} \nu h_3 e_1 - \frac{n \nu}{\Omega_0} e_1, \quad (92)$$

$$e_3' = \frac{1 - 4 \nu}{2} h_1 e_2 - \frac{1 + 4 \nu}{2} h_2 e_1. \quad (93)$$

Substituting $\nu = 0$, the readers may recover the correct form of the Galactic disc tide equations published in Breiter & Ratajczak (2005, 2006). Equations (88)–(93) admit three integrals of motion: apart from the usual conservation of the time-independent Hamiltonian $\mathcal{K} = \text{constant}$, two geometrical constraints

$$\mathbf{h} \cdot \mathbf{e} = 0, \quad h^2 + e^2 = 1, \quad (94)$$

are respected thanks to the properties of the Lie–Poisson bracket (81). Indeed, both quadratic forms are the Casimir functions of our bracket, i.e.

$$(\mathbf{h} \cdot \mathbf{e}; f) = (h^2 + e^2; f) = 0, \quad (95)$$

for any function f , hence for $f = \mathcal{K}$ in particular.

3.2 Lie–Poisson splitting method

Hamiltonian \mathcal{K} can be split into a sum of three non-commuting terms

$$\mathcal{K} = \mathcal{K}_1 + \mathcal{K}_2 + \mathcal{K}_3, \quad (96)$$

$$\mathcal{K}_1 = \frac{5}{4} \nu e_1^2 - \frac{1+\nu}{4} h_1^2, \quad (97)$$

$$\mathcal{K}_2 = -\frac{5}{4} \nu e_2^2 - \frac{1-\nu}{4} h_2^2, \quad (98)$$

$$\mathcal{K}_3 = -\frac{5}{4} e_3^2 + \frac{n\nu}{\Omega_0} h_3. \quad (99)$$

Each of the terms \mathcal{K}_i is in turn a sum of two components that commute, because it can be easily verified that $(e_j; h_j) = 0$ for all $j \in \{1, 2, 3\}$. In these circumstances, we can approximate the real solution

$$\mathbf{v}(\tau) = \exp(\tau L) \mathbf{v}(0), \quad (100)$$

where $L f \equiv (f; \mathcal{K})$, using a composition of maps

$$\Psi_{i,\tau} : \mathbf{v}(0) \rightarrow \mathbf{v}(\tau) = \exp(\tau L_i) \mathbf{v}(0), \quad (101)$$

where $L_i f \equiv (f; \mathcal{K}_i)$, for $i = 1, 2, 3$. Each $\Psi_{i,\tau}$ is in turn a composition of two maps

$$\Psi_{i,\tau} = E_{i,\tau} \circ H_{i,\tau} = H_{i,\tau} \circ E_{i,\tau}, \quad (102)$$

generated by the e_i and h_i related terms of \mathcal{K}_i .

3.2.1 The contribution of \mathcal{K}_1

The two terms of \mathcal{K}_1 generate equations of motion

$$\mathbf{v}' = \left(\mathbf{v}; \frac{5}{4} \nu e_1^2 \right) = \frac{5}{2} e_1 \nu \begin{pmatrix} \mathbf{0} & \mathbf{Y}_1 \\ \mathbf{Y}_1 & \mathbf{0} \end{pmatrix} \mathbf{v}, \quad (103)$$

and

$$\mathbf{v}' = \left(\mathbf{v}; -\frac{1}{4}(1+\nu)h_1^2 \right) = -\frac{1}{2} h_1 (1+\nu) \begin{pmatrix} \mathbf{Y}_1 & \mathbf{0} \\ \mathbf{0} & \mathbf{Y}_1 \end{pmatrix} \mathbf{v}, \quad (104)$$

where

$$\mathbf{Y}_1 = \begin{pmatrix} 0 & 0 & 0 \\ 0 & 0 & 1 \\ 0 & -1 & 0 \end{pmatrix}. \quad (105)$$

Introducing

$$c_{ij} = \cos \psi_{ij}, \quad s_{ij} = \sin \psi_{ij}, \quad (106)$$

we can write their solutions as

$$E_{1,\tau} : \mathbf{v} \rightarrow \begin{pmatrix} h_1 \\ h_2 c_{11} + e_3 s_{11} \\ h_3 c_{11} - e_2 s_{11} \\ e_1 \\ e_2 c_{11} + h_3 s_{11} \\ e_3 c_{11} - h_2 s_{11} \end{pmatrix}, \quad (107)$$

with

$$\psi_{11} = \frac{5}{2} e_1 \nu \tau, \quad (108)$$

and

$$H_{1,\tau} : \mathbf{v} \rightarrow \begin{pmatrix} h_1 \\ h_2 c_{12} - h_3 s_{12} \\ h_3 c_{12} + h_2 s_{12} \\ e_1 \\ e_2 c_{12} - e_3 s_{12} \\ e_3 c_{12} + e_2 s_{12} \end{pmatrix}, \quad (109)$$

where

$$\psi_{12} = \frac{1}{2} (1+\nu) h_1 \tau. \quad (110)$$

The composition of these two maps results in

$$\Psi_{1,\tau} : \mathbf{v} \rightarrow \begin{pmatrix} \mathbf{M}_1 & \mathbf{N}_1 \\ \mathbf{N}_1 & \mathbf{M}_1 \end{pmatrix} \mathbf{v}, \quad (111)$$

where

$$\mathbf{M}_1 = \begin{pmatrix} 1 & 0 & 0 \\ 0 & c_{11}c_{12} & -c_{11}s_{12} \\ 0 & c_{11}s_{12} & c_{11}c_{12} \end{pmatrix}, \quad (112)$$

$$\mathbf{N}_1 = \begin{pmatrix} 0 & 0 & 0 \\ 0 & s_{11}s_{12} & s_{11}c_{12} \\ 0 & -s_{11}c_{12} & s_{11}s_{12} \end{pmatrix}. \quad (113)$$

3.2.2 The contribution of \mathcal{K}_2

The equations of motion derived from the two terms of \mathcal{K}_2 are

$$\mathbf{v}' = \left(\mathbf{v}; -\frac{5}{4} \nu e_2^2 \right) = \frac{5}{2} \nu e_2 \begin{pmatrix} \mathbf{0} & \mathbf{Y}_2 \\ \mathbf{Y}_2 & \mathbf{0} \end{pmatrix} \mathbf{v}, \quad (114)$$

and

$$\mathbf{v}' = \left(\mathbf{v}; -\frac{1}{4}(1-\nu)h_2^2 \right) = \frac{1}{2} (1-\nu) h_2 \begin{pmatrix} \mathbf{Y}_2 & \mathbf{0} \\ \mathbf{0} & \mathbf{Y}_2 \end{pmatrix} \mathbf{v}, \quad (115)$$

where

$$\mathbf{Y}_2 = \begin{pmatrix} 0 & 0 & 1 \\ 0 & 0 & 0 \\ -1 & 0 & 0 \end{pmatrix}. \quad (116)$$

Their solutions are

$$E_{2,\tau} : \mathbf{v} \rightarrow \begin{pmatrix} h_1 c_{21} + e_3 s_{21} \\ h_2 \\ h_3 c_{21} - e_1 s_{21} \\ e_1 c_{21} + h_3 s_{21} \\ e_2 \\ e_3 c_{21} - h_1 s_{21} \end{pmatrix}, \quad (117)$$

where

$$\psi_{21} = \frac{5}{2} \nu e_2 \tau, \quad (118)$$

and

$$H_{2,\tau} : v \rightarrow \begin{pmatrix} h_1 c_{22} - h_3 s_{22} \\ h_2 \\ h_3 c_{22} + h_1 s_{22} \\ e_1 c_{22} - e_3 s_{22} \\ e_2 \\ e_3 c_{22} + e_1 s_{22} \end{pmatrix}, \quad (119)$$

where

$$\psi_{22} = -\frac{h_2(1-\nu)}{2} \tau. \quad (120)$$

Composing the two maps, we obtain

$$\Psi_{2,\tau} : v \rightarrow \begin{pmatrix} \mathbf{M}_2 & \mathbf{N}_2 \\ \mathbf{N}_2 & \mathbf{M}_2 \end{pmatrix} v, \quad (121)$$

where

$$\mathbf{M}_2 = \begin{pmatrix} c_{21}c_{22} & 0 & -c_{21}s_{22} \\ 0 & 1 & 0 \\ c_{21}s_{22} & 0 & c_{21}c_{22} \end{pmatrix}, \quad (122)$$

$$\mathbf{N}_2 = \begin{pmatrix} s_{21}s_{22} & 0 & c_{22}s_{21} \\ 0 & 0 & 0 \\ -c_{22}s_{21} & 0 & s_{21}s_{22} \end{pmatrix}. \quad (123)$$

3.2.3 The contribution of \mathcal{K}_3

The equations of motion derived from the two terms of \mathcal{K}_3 are

$$v' = \left(v; -\frac{5}{4} e_3^2 \right) = \frac{5}{2} e_3 \begin{pmatrix} \mathbf{0} & \mathbf{Y}_3 \\ \mathbf{Y}_3 & \mathbf{0} \end{pmatrix} v, \quad (124)$$

and

$$v' = \left(v; h_3 n \nu \Omega_0^{-1} \right) = -\frac{n \nu}{\Omega_0} \begin{pmatrix} \mathbf{Y}_3 & \mathbf{0} \\ \mathbf{0} & \mathbf{Y}_3 \end{pmatrix} v, \quad (125)$$

where

$$\mathbf{Y}_3 = \begin{pmatrix} 0 & -1 & 0 \\ 1 & 0 & 0 \\ 0 & 0 & 0 \end{pmatrix}. \quad (126)$$

Their solutions are

$$E_{3,\tau} : v \rightarrow \begin{pmatrix} h_1 c_{31} - e_2 s_{31} \\ h_2 c_{31} + e_1 s_{31} \\ h_3 \\ e_1 c_{31} - h_2 s_{31} \\ e_2 c_{31} + h_1 s_{31} \\ e_3 \end{pmatrix}, \quad (127)$$

where

$$\psi_{31} = \frac{5}{2} e_3 \tau, \quad (128)$$

and

$$H_{3,\tau} : v \rightarrow \begin{pmatrix} h_1 c_{32} + h_2 s_{32} \\ h_2 c_{32} - h_1 s_{32} \\ h_3 \\ e_1 c_{32} + e_2 s_{32} \\ e_2 c_{32} - e_1 s_{32} \\ e_3 \end{pmatrix}, \quad (129)$$

where

$$\psi_{32} = \frac{n \nu}{\Omega_0} \tau. \quad (130)$$

Composing the two maps, we obtain

$$\Psi_{3,\tau} : v \rightarrow \begin{pmatrix} \mathbf{M}_3 & \mathbf{N}_3 \\ \mathbf{N}_3 & \mathbf{M}_3 \end{pmatrix} v, \quad (131)$$

where

$$\mathbf{M}_3 = \begin{pmatrix} c_{31}c_{32} & c_{31}s_{32} & 0 \\ -c_{31}s_{32} & c_{31}c_{32} & 0 \\ 0 & 0 & 1 \end{pmatrix}, \quad (132)$$

$$\mathbf{N}_3 = \begin{pmatrix} s_{31}s_{32} & -c_{32}s_{31} & 0 \\ c_{32}s_{31} & s_{31}s_{32} & 0 \\ 0 & 0 & 0 \end{pmatrix}. \quad (133)$$

3.3 Tangent map

In order to follow the evolution of a tangent vector δ , we linearize the maps $\Psi_{i,\tau}$, obtaining

$$D\Psi_{i,\tau} : \delta \rightarrow \begin{pmatrix} \mathbf{M}_i & \mathbf{N}_i \\ \mathbf{N}_i & \mathbf{M}_i \end{pmatrix} \delta + (\delta_{i+3} \mathbf{Q}_{i,1} + \delta_i \mathbf{Q}_{i,2}) v, \quad (134)$$

where

$$\mathbf{Q}_{i,1} = \frac{\partial \psi_{i1}}{\partial e_i} \frac{\partial}{\partial \psi_{i1}} \begin{pmatrix} \mathbf{M}_i & \mathbf{N}_i \\ \mathbf{N}_i & \mathbf{M}_i \end{pmatrix}, \quad (135)$$

and

$$\mathbf{Q}_{i,2} = \frac{\partial \psi_{i2}}{\partial h_i} \frac{\partial}{\partial \psi_{i2}} \begin{pmatrix} \mathbf{M}_i & \mathbf{N}_i \\ \mathbf{N}_i & \mathbf{M}_i \end{pmatrix}. \quad (136)$$

The resulting expressions are easy to derive (even by hand), so we do not quote them explicitly.

Choosing the initial value of the tangent vector δ is a more subtle task for the Lie–Poisson system than it was for the canonical KS integrator. Not only we want to set up δ orthogonal to the flow, i.e.

$$\delta \cdot (v; \mathcal{K}) = 0, \quad (137)$$

but we also aim at respecting the properties (94), which means

$$\delta \cdot v = 0, \quad (138)$$

$$\delta_1 e_1 + \delta_2 e_2 + \delta_3 e_3 = -\delta_4 h_1 - \delta_5 h_2 - \delta_6 h_3. \quad (139)$$

Let us select

$$\delta = \begin{pmatrix} \mathbf{h} \times (\mathbf{h}; \mathcal{K}) + \mathbf{e} \times (\mathbf{e}; \mathcal{K}) \\ \mathbf{h} \times (\mathbf{e}; \mathcal{K}) + \mathbf{e} \times (\mathbf{h}; \mathcal{K}) \end{pmatrix}. \quad (140)$$

Recalling the definition of the Lie–Poisson bracket (81), one can easily verify that regardless of the form of \mathcal{K} this choice satisfies all three requests: (137), (138) and (139).

3.4 Higher order methods. General properties

The composition methods of Laskar & Robutel (2001) cannot be used for our Lie–Poisson splitting method, because the Hamiltonian function has been partitioned into three terms. Moreover, none of the terms can be qualified as a small perturbation. In these circumstances, the principal building block can be a ‘generalized leapfrog’

$$\Psi_{\Delta} = \Psi_{1,\Delta/2} \circ \Psi_{2,\Delta/2} \circ \Psi_{3,\Delta} \circ \Psi_{2,\Delta/2} \circ \Psi_{1,\Delta/2}. \quad (141)$$

This LPV2 method is a second-order method with a local truncation error proportional to the cube of the step size Δ^3 . A similar composition method can be applied to the tangent map, with all Ψ in (141) replaced by $D\Psi$. Although we use LPV2 as a final product in this paper, it can be used as a building block for higher order methods. A collection of appropriate composition rules can be found in McLachlan & Quispel (2002).

4 NUMERICAL TESTS

4.1 Laskar–Robutel composition methods

Our final choice of BABC3 method of Laskar & Robutel (2001) in LARKS has been the result of a series of accuracy tests involving various BABN (without corrector) and BABCN (with corrector) composition rules for $N = 1, 2, 3, 4$. As the accuracy measure, we used the conservation of the time-independent Hamiltonian function (68), reflected in the relative error parameter, i.e. the maximal error along the trajectories given by

$$E(t) = \max_{0 \leq \tau \leq t} \left| \frac{\mathcal{H}(\tau) - \mathcal{H}(t_0)}{\mathcal{H}(t_0)} \right|. \quad (142)$$

In principle, the truncation error of the Hamiltonian function in splitting methods should be proportional to the local truncation error of variables divided by the first power of step size.

Two fictitious comets were studied: one with $a_0 = 30\,000$ au, and one with the initial semi-axis $a_0 = 50\,000$ au. The remaining orbital elements were $e_0 = 0.1$, $i_0 = 80^\circ$ and $\omega_0 = 110^\circ$; both the ascending node longitude and the mean anomaly were set to 0. The motion of the test bodies was integrated over 500 orbital periods, with the time-steps corresponding approximately to P_0/k , where P_0 is the initial orbital period of the comet and for $2 \leq k \leq 1000$. Orbital evolution of the two test bodies is different: the one with a smaller semi-axis reached the maximum eccentricity $e \approx 0.22$, whereas the osculating eccentricity of the second body was periodically reaching $e \approx 0.98$. Using the maximum values of the ratio $|\mathcal{H}_1/\mathcal{H}_0|$ to estimate ε , we found $\varepsilon \approx 0.01$ and $\varepsilon \approx 0.04$ for the two comets, respectively. The ratio of these values is 0.25, in a good agreement with the rule of thumb $\varepsilon \propto a^3$ that leads to the ratio $(3 \times 10^4/5 \times 10^4)^3 \approx 0.22$.

The error values of different composition methods versus the number of time-step per orbital period, and those versus the computational time needed for each integration are shown in Fig. 1. Inspecting the step size dependence of various methods, we find three characteristic slopes present to the left of Fig. 1; they refer to the errors of the Hamiltonian proportional to N^{-2} (all BABs and BABC1), or N^{-4} (BABC2, BABC3 and BABC4) for both orbits. These features indicate that all uncorrected integrators are indeed second-order methods, although BAB1 has the error of the Hamiltonian proportional to Δ^2 , whereas remaining methods have the error term in the form $\varepsilon \Delta^2$, where Δ is the time-step and ε the ratio of the perturbing term to the Keplerian Hamiltonian. Obviously, adding corrector to BAB1 is useless, because suppressing the $\varepsilon \Delta^2$ term

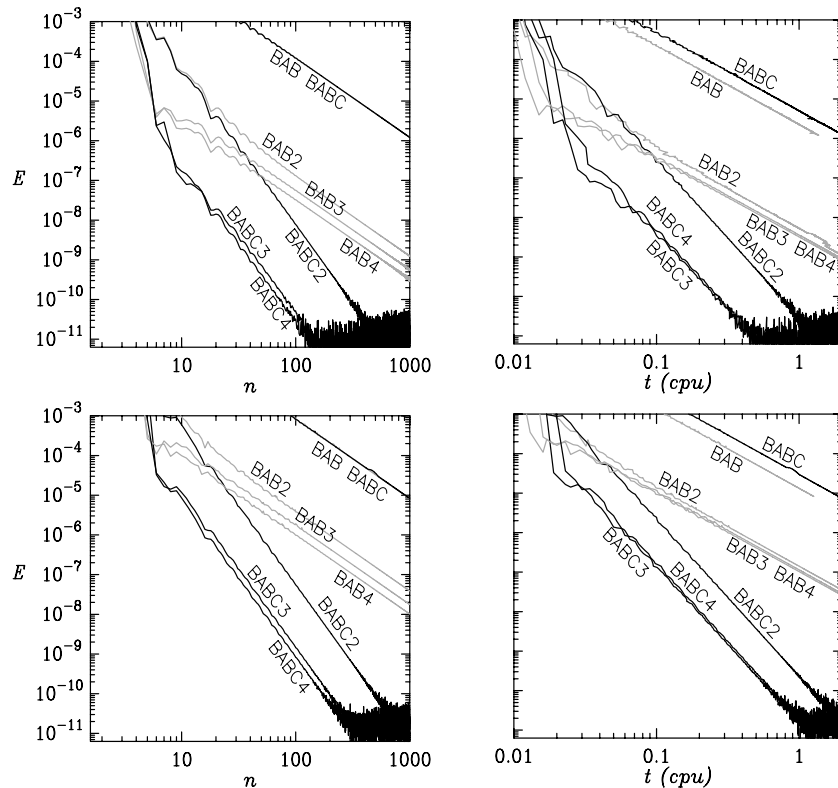


Figure 1. Relative error E of the Hamiltonian over 500 orbital periods versus the number of steps per period (left) and the computational time (right) for a 30 000 au comet (top) and a 50 000 au comet (bottom). Black curves correspond to integrators without corrector, grey curves – integrators with corrector.

has no influence on the results. Other integrators are successfully upgraded by corrector, attaining the $\varepsilon^2 \Delta^4$ error in good agreement with the formal estimates of Laskar & Robutel (2001).

Considering only the models with corrector, we note in Fig. 1 that BABC3 and BABC4 have almost the same accuracy and computation time. In these circumstances, we choose BABC3 as the method with less intermediate stages.

4.2 Hamiltonian mapping versus new integrators

Let us compare the efficiency of the regularized symplectic integrators with the Hamiltonian mappings introduced in Fouchard (2004) and developed in Fouchard et al. (2005, 2006). The latter are built as the Taylor series solution of the canonical equations of motion averaged with respect to the comet's mean anomaly. The final model which is described in Fouchard et al. (2006) will be referred to as the MAPP model.

We have also programmed a symplectic integrator using a similar fictitious time as LARKS, but working in Cartesian coordinates and momenta. This MIKLAR (Mikkola–Laskar–Robutel) code uses the recipes compiled from Mikkola (1997), Preto & Tremaine (1999), Mikkola & Wiegert (2002) and Mikkola, Palmer & Hashida (2002). It is based on the Hamiltonian function

$$\mathcal{N} = r \left(\mathcal{H}(x, y, z, t, X, Y, Z) + X^* \right) = 0, \quad (143)$$

where \mathcal{H} is given by equations (1)–(7), split into the Keplerian part and the perturbation. The extended phase space has a lower dimension than in KS variables (8 as compared to 10), but the ‘exact leapfrog’ (Preto & Tremaine 1999; Mikkola & Wiegert 2002) used in the Keplerian map is computationally more costly than in the KS case. The repetition of the tests for various Laskar–Robutel composition methods that are discussed in Section 4.1 resulted in the results very similar to LARKS. The accuracy curves for MIKLAR occurred to be very close to their LARKS counterparts shown in Fig. 1, with the agreement on the level of few percents. One may conclude that, at least in the problem discussed here, it is the time regularization that plays a fundamental role; using the KS variables or the Cartesian coordinates is merely a question of an arbitrary choice. In these circumstances, we choose the LARKS integrator.

4.2.1 Test problem

In order to compare the reliability and speed of the integrators, we performed the following experiment. 400 000 of initial orbital elements were randomly chosen in a specified range, under the condition that their respective distribution is uniform, i.e.:

- (i) the initial semimajor axes are in the range $3000 \leq a_0 \leq 10^5$ au, such as their distribution is uniform in $\log_{10} a_0$;
- (ii) the initial eccentricity is in the range $0 \leq e_0 \leq 0.9999$, with a uniform distribution;
- (iii) the initial inclination i_0 is such that $-1 \leq \cos i_0 \leq 1$, with a uniform distribution;
- (iv) the initial argument of the perihelion, the longitude of the ascending node, and the initial mean anomaly (where needed) in the range from 0 to 2π , with a uniform distribution.

Using this set of elements, we integrated the equations over one cometary period using LARKS, MIKLAR, LPV2, MAPP and confronting the results with the ones obtained by the Radau–Everhart RA15 integrator of the order of 15 (Everhart 1985) with the automatic step size choice imposed by $LL = 12$. The relative error in

comet's position E_p was defined as

$$E_p = \left| \frac{q_{\text{mod}} - q_R}{q_0} \right|, \quad (144)$$

where q_{mod} , and q_R denote the value of the perihelion distance at the end of the integration of one period computed by the tested integrator and by the RA15, respectively, and q_0 is the initial value of the perihelion distance.

Then, the e_0 – $\log_{10} a_0$ plane is divided into 60×70 cells. In each cell, we record the maximum value E_{max} reached by the error E_p for the initial conditions belonging to the cell.

4.2.2 LARKS step size choice

As we know from Fig. 1, the Hamiltonian error of LARKS, based on the BABC3 composition, is proportional to $\varepsilon^2 \Delta^4$. Observing that $\varepsilon \propto a^3$, where a is the semimajor axis of a comet, we look for the step size selection rule that renders a similar precision for a wide range of initial conditions. This can be achieved if the product

$$K = \varepsilon^2 \Delta^4, \quad (145)$$

has similar values for all comets to be studied. Thus, finding some optimum step size Δ_0 for a given semi-axis a_0 , and then launching the integration for a different semi-axis a_1 , we adjust the step size and use

$$\Delta_1 = \Delta_0 \left(\frac{a_0}{a_1} \right)^{3/2}. \quad (146)$$

In the test described in this section, we set Δ_0 as 1/20 of the Keplerian period implied by $a_0 = 50\,000$ au and adjusted the step according to (146) for other orbits. However, in order to avoid numerical resonance between the step size and orbital period (Wisdom & Holman 1992), we do not use the step size larger than 1/20 of the Keplerian period, even if it might result from equation (146).

4.2.3 Stop time for LARKS

Fictitious time τ as the independent variable is an inevitable point of the KS variables regularization. However, what if we aim to obtain the state of a comet at some particular final epoch of the physical time t ? This problem appeared in our tests, because we wanted to stop the integration as close as possible to the real orbital period of the comet T_f . Let $(\mathbf{u}_p, \mathbf{U}_p)$ and t_p be the KS variables and physical time before some step, and $(\mathbf{u}_a, \mathbf{U}_a)$ and t_a – after this step. We stopped the integration as soon as $t_a \geq T_f$. Then, we performed an additional step from the closest position to final one using a fictitious time-step equal to $\Delta(T_f - t_c)/(t_a - t_i)$, where Δ is the previous step size and $t_c = t_p$ or t_a , depending on which epoch was closer to the final one. After this stage, we used the approximate rule

$$\Delta \approx \frac{\alpha^2}{4 \mathbf{u}^2} (T_f - t),$$

iterated until $|T_f - t| < 1$ yr. Such precision is generally obtained within two iterations; consequently the computational cost needed to reach to correct final position was negligible.

4.2.4 Final results

The results obtained for the three models are shown in Fig. 2. The MAPP and the LPV2 models, both used with a step size equal to the unperturbed Keplerian period, are equivalent as the accuracy is

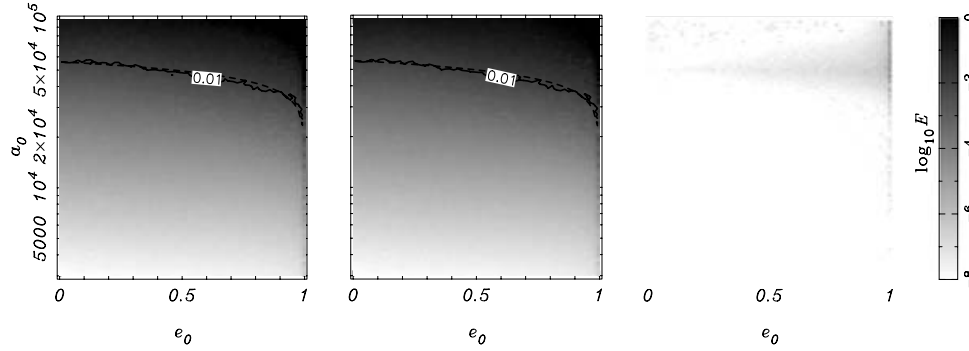


Figure 2. Maximum error \bar{E}_p (see equation 144) in each cell of the e_0 – a_0 plane for the models MAPP (left), LPV2 (middle) and LARKS (right). The solid line curves correspond to $E_p = 0.01$ and the dotted curves are the best fits of the level curves.

concerned. Indeed, the best analytical fit of the level curve $E_p = 0.01$ is given by

$$a_c = 10^{4.748 \pm 0.004} (1 - e)^{0.182 \pm 0.006}, \quad (147)$$

for the MAPP model and,

$$a_c = 10^{4.751 \pm 0.003} (1 - e)^{0.185 \pm 0.005}, \quad (148)$$

for the LPV2 model. These two equations may be considered as identical within the error bounds of the exponents.

For both models the error is essentially due to the averaging of the equations of motion with respect to the mean anomaly. Conversely, the LARKS method is highly reliable in the whole phase-space domain under study, since the error never exceeds 0.01. The effect of the time-step selection rule (146) is clearly visible above $a_0 = 50\,000$ au; the reliability of LARKS is almost conserved when a_0 increases.

Speaking about the computation times required to perform all the integrations, the MAPP, LPV2 and LARKS needed 5.5, 1.8 and 75 s, whereas the RA15 integration took 1820 s. Consequently, LPV2 is three times faster than MAPP, and almost 40 times faster than LARKS. All the timing tests were performed without the propagation of the variations vector. Including the tangent maps doubles the computation time for LARKS and MIKLAR with SBABC3 (factors of 2.4 and 2.2, respectively), due to the computation of the tangent Kepler maps (four times per step) and of the tangent perturbation maps (five times per step instead of two usually required for the corrector). The difference in computation time with and without the propagation of variations for LPV2 is smaller (factor of 1.7), thanks to the simplicity of the tangent maps expressions. The difference is even smaller for MAPP (about 1.01) because, based on the Taylor series, it evaluates the Jacobian of the right-hand sides anyway.

5 CONCLUSIONS

The two integrators presented in this paper are fast and reliable. Their application range is complementary in two aspects. First, according to the results of Section 4.2.4, we can use LPV2 below the $E_p = 0.01$ level curve (or its analytical fit given by equation 148), and LARKS above this level curve. This aggregate allows a fast simulation of numerous cometary samples within the assumed 1 per cent accuracy bound. The integrators are also complementary, because if we generate two maps of a chaos indicator values (one with LARKS, and one with LPV), their comparison will immediately show which chaotic zones are due to secular resonances and

which come from the mean motion resonance. The results of such studies will be published in a separate paper. We can already announce that the results of our simulations using the new tools are coherent with that of Brassier (2001).

ACKNOWLEDGMENTS

The authors appreciate helpful suggestions of Prof. Jacques Laskar concerning the idea and details of using symplectic integrators in the present framework. An anonymous reviewer helped us considerably to improve the paper. MF is grateful to ESA for financial support at INAF–IASF.

REFERENCES

- Barrio R., 2005, *Chaos Solitons Fractals*, 25, 711
 Brassier R., 2001, *MNRAS*, 324, 1109
 Breiter S., 1998, *Celest. Mech. Dyn. Astron.*, 71, 229
 Breiter S., Ratajczak R., 2005, *MNRAS*, 364, 1222
 Breiter S., Ratajczak R., 2006, *MNRAS*, 367, 1808
 Deprit A., Elpe A., Ferrer S., 1994, *Celest. Mech. Dyn. Astron.*, 58, 151
 Everhart E., 1985, in Carusi A., Valsecchi G. B., eds, *ASSL Vol. 115*, IAU Colloq. 83, *Dynamics of Comets: Their Origin and Evolution*. p. 185
 Fouchard M., 2004, *MNRAS*, 349, 347
 Fouchard M., Froeschlé C., Matese J. J., Valsecchi G., 2005, *Celest. Mech. Dyn. Astron.*, 93, 229
 Fouchard M., Froeschlé C., Valsecchi G., Rickman H. 2006, *Celest. Mech. Dyn. Astron.*, 95, 299
 Laskar J., Robutel P., 2001, *Celest. Mech. Dyn. Astron.*, 80, 39
 Levison H. F., Dones L., Duncan M. J., 2001, *AJ*, 121, 2253
 McLachlan R. I., Quispel G. R. W., 2002, *Acta Numer.*, 11, 341
 Mikkola S., 1997, *Celest. Mech. Dyn. Astron.*, 67, 145
 Mikkola S., Innanen K., 1999, *Celest. Mech. Dyn. Astron.*, 74, 59
 Mikkola S., Wiegert P., 2002, *Celest. Mech. Dyn. Astron.*, 82, 375
 Mikkola S., Palmer P., Hashida Y., 2002, *Celest. Mech. Dyn. Astron.*, 82, 391
 Preto M., Tremaine S., 1999, *AJ*, 118, 2532
 Stiefel E. L., Scheifele G., 1971, *Linear and Regular Celestial Mechanics*. Springer-Verlag, Berlin
 Szebehely V., 1967, *Theory of Orbits: The Restricted Problem of Three Bodies*. Academic Press, New York
 Wisdom J., Holman M., 1992, *AJ*, 104, 2022
 Wisdom J., Holman M., Touma J., 1996, *Integration Algorithms and Classical Mechanics*. AMS, Providence, RI, p. 217

This paper has been typeset from a $\text{\TeX}/\text{\LaTeX}$ file prepared by the author.